Article

A Co-Powered Biomass and Concentrated Solar Power Rankine Cycle Concept for Small Size Combined Heat and Power Generation

Domenico Borello [1], Alessandro Corsini [2], Franco Rispoli [1] and Eileen Tortora [1,]*

[1] Dipartimento di Meccanica e Aeronautica, Sapienza Università di Roma, Via Eudossiana 18, 00184, Roma, Italy; E-Mails: domenico.borello@uniroma1.it (D.B.); franco.rispoli@uniroma1.it (F.R.)

[2] Facoltà di Ingegneria, Sapienza Università di Roma, Via Andrea Doria 3, 04100, Latina, Italy; E-Mail: alessandro.corsini@uniroma1.it

* Author to whom correspondence should be addressed; E-Mail: eileen.tortora@uniroma1.it; Tel.: +39-064-458-523-1; Fax: +39-064-458-5250.

Abstract: The present work investigates the matching of an advanced small scale Combined Heat and Power (CHP) Rankine cycle plant with end-user thermal and electric load. The power plant consists of a concentrated solar power field co-powered by a biomass furnace to produce steam in a Rankine cycle, with a CHP configuration. A hotel was selected as the end user due to its high thermal to electric consumption ratio. The power plant design and its operation were modelled and investigated by adopting transient simulations with an hourly distribution. The study of the load matching of the proposed renewable power technology and the final user has been carried out by comparing two different load tracking scenarios, *i.e.*, the thermal and the electric demands. As a result, the power output follows fairly well the given load curves, supplying, on a selected winter day, about 50 GJ/d of thermal energy and the 6 GJ/d of electric energy, with reduced energy dumps when matching the load.

Keywords: co-powered concentrated solar power; Rankine cycle; transient simulation; load matching

Nomenclature

E_{el}	Electric energy output (GJ)
$E_{el,d}$	Electric energy demand (GJ)
E_g	Global energy input from biomass and solar radiation (GJ)
E_{th}	Thermal energy output (GJ)
$E_{th,d}$	Thermal energy demand (GJ)
h	Enthalpy (kJ/kg)
$\dot{m}_F$	HTF flow rate (m^3/h)
$\dot{m}_{F,CSP}$	Solar field HTF delivered flow rate (m^3/h)
$\dot{m}_{F,bmin}$	Minimum biomass furnace HTF delivered flow rate (m^3/h)
$\dot{m}_{F,b+}$	Additional biomass furnace HTF delivered flow rate (m^3/h)
$\dot{m}_{F,d}$	HTF demanded flow rate (m^3/h)
$\dot{m}_{F,s}$	Solar direct and TES delivered flow rate (m^3/h)
$\dot{m}_{F,TESc}$	TES HTF charge flow rate (m^3/h)
$\dot{m}_{F,TESd}$	TES HTF discharge flow rate (m^3/h)
P	Pressure (bar)
P_b	Biomass derived power (kW)
$P_{b,min}$	Biomass furnace power at minimum duty (kW)
P_{CSP}	CSP derived thermal power (kW)
P_{eg}	Exhaust gas power (kW)
P_{el}	Electric power output (kW)
$P_{el,d}$	Electric load power (kW)
$P_{TES,c}$	Storage charge power (kW)
$P_{TES,d}$	Storage discharge power (kW)
P_{th}	Thermal power output (kW)
$P_{th,d}$	Thermal load power (kW)
s	Entropy (kJ/kg °C)
T	Temperature (°C)
x	Vapour fraction (-)
δ	Density (kg/m^3)
η_{el}	Reference electric efficiency (-)
η_{th}	Reference thermal efficiency (-)

1. Introduction

In recent years the use of Combined Heat and Power (CHP) was commonly considered to supply energy to end users in the service or residential sectors. The basic argument in favour of CHP is the possibility to obtain electric and thermal energy *in situ*, improving the power generation efficiency and reducing the losses usually related to the energy distribution [1,2]. Notably among the existing CHP

technologies, only a few exceptions are based on the exploitation of different fuels from natural gas, *i.e.*, small-scale power plants based on biomass derived fuel exploitation, like wood or biogas [3].

In most applications the main factor determining the economic viability of CHP schemes is the high utilisation of heat and electric energy, which are produced simultaneously. Most of the literature indicates that a CHP plant needs to be fully utilised providing heat and power for a minimum duty of 4,500 h per annum to attain its breakeven point [4].

When designing renewable energy-based CHP technologies, in a distributed generation concept, one of the key factors is the capability of tracking the time-dependent end-user load. Given the unpredictability of weather conditions, renewable energy systems often rely on energy backup systems to assure that the load demands are met by the overall system.

Several solutions have been proposed to attenuate the RES-user matching inconsistency. The conventional remedial strategy is to plug the supply gap providing alternative capacity, known as spinning reserve [5]. Among the solutions devoted to RES electric grid integration, it is worth mentioning the use of high capacity energy storage to save the produced energy surplus and postponing the energy surplus delivery [6,7], or combining renewable energy sources with complementary intermittencies [8].

The present study investigates a CHP scheme combining a parabolic trough field for concentrated solar power (CSP), a thermal energy storage and a biomass furnace as complementary source. It is worth noting that the biomass source allows to easily store the energy source as far as produce instant power, alike conventional fossil fuel based systems.

The parabolic trough field was selected for its high worldwide development among current CSP systems [9]. An important aspect of these plants is the size, which is usually large. In fact solar trough plants are characterized by multi-MW sizes, which range up to about 50 MW_{el} for parabolic trough systems. Nevertheless, recently the interest in small and medium scale solar plant has increased, aiming to supply heat to the industrial sector in the 100–400 °C range by using the existing concentrated solar power technologies [10]. The biomass power plants are also usually rated in the 5–100 MW range. Even so, while CSP plants size is still growing [11,12], in the biomass field there are several applications on small-scale biomass power plants [13,14].

The aim to exploit CSP technology and limit the plant footprint led to the design of a small scale plant, recently presented in [15], composed by a 2,580 m^2 parabolic trough field, a thermal energy storage system (TES) and a 1,163 kW biomass furnace to respond to the solar source fluctuations. A heat transfer fluid (HTF), *i.e.*, a diathermic oil, is heated by the parabolic through a field and biomass furnace and subsequently it is sent to a heat recovery steam generator where it produces low enthalpy saturated steam that is sent to a 130 kW reciprocating steam engine for the electric energy production. Moreover, the Rankine cycle (RC) economizer is fed by the exhaust gases derived from the biomass combustion. A heat recovery for thermal energy production is obtained, using hot water as heat carrier, in a back-pressure scheme at 134 °C and 300 kPa. The heat recovery system was designed in order to be able to produce also supercritical steam at medium temperature (up to 100 °C).

The proposed RES based small scale CHP Rankine cycle plant was matched to a typical hostelry end user. The tertiary sector, including hotels, has been identified by the European Union Action Plan for Energy, as the sector with the higher savings potential (30%) by 2020, with respect to household sector (27%), transports (26%) and manufacturing industry (25%). For instance, hotels show a typical

annual power consumption of 350 kWh/m^2 [16], sensibly higher than that of normal commercial buildings (30–152 kWh/m^2) [17]. It is evident that a deep intervention on the energy request and on the kind of energy supply for the hotel sector leads to a faster achievement of the GHG reduction goals. Although the application of a CHP plant appears interesting as the preponderance of the thermal power production with respect to the electric one perfectly matches with the high heat/electricity consumption ratio of the hotels, only few studies deal with the application of CHP to hotel energy requests, aiming to assess methods to estimate the best capacity and operation strategy [18,19] and the economic feasibility [20]. To the best of the authors' knowledge, only one study can be found in the literature dealing with a renewable based CHP for hotel application, taking into account solar photovoltaic and biomass gasification technologies [21].

The system matching behaviour is analyzed for both thermal and electric load tracking with the aim to demonstrate its capability to meet the end-users energy request on a 24 hour period in a winter day as more challenging for the solar field performance.

The investigation of the matching between the proposed plant and the end user was carried out by transient model simulations. The transient model and the simulations were performed in the TRNSYS environment [22] supported by the in-house made types of the biomass furnace and reciprocating steam engine and the STEC component model library [23]. The software TRNSYS was selected as it is a well-known instrument to model complex energy systems, as demonstrated by several studies appeared in the open literature which mostly deal on RES applications in a few fields like small-islands stand alone power systems [7,24], or, more related to the present paper, on CSP field simulations [25,26], TES behaviour in solar trough plants [27] and matching to a hotel end-user [15].

2. Co-Powered Solar-Biomass Plant and Model Description

2.1. Component and System Description

The proposed CHP concept, Figure 1, consists of an integrated solar-biomass Rankine cycle system. The basic equipment of the power block consists of a 1,200 kW solar trough field, 57 GJ thermal energy storage at full load (26 h capacity) and 1,163 kW biomass furnace to feed the heat transfer fluid loop and the related RC. Although biofuel can be easily stored and it is promptly available, the TES allows one to avoid the surplus CSP energy dump occurring in situations of overproduction. In this way the stored energy can be used in deficit situations, recurring to the biomass only as a second option.

It is worth noting that the biomass furnace is constantly on duty at a minimum power (*i.e.*, the 35% of its maximum power, 407 kW$_{th}$), in order to ease its complementary source role avoiding power output deficits and/or furnace start-up problems related to the Direct Normal Insulation (DNI) sudden variations.

The HTF circuit supplies the thermal energy to the RC for the production of saturated steam to be expanded in a 130 kW reciprocating steam engine coupled with an electric generator. The expanded steam is condensed producing a thermal power output available at a constant temperature of 80 °C, *i.e.*, the temperature demand of typical district heating networks. As stated before, the condensing temperature of the RC is sensibly higher than the demanded temperature in order to allow the sporadic

production of superheated steam. The main components and system thermodynamic parameters, subdivided in diathermic oil and water/steam circuit, are described in Table 1.

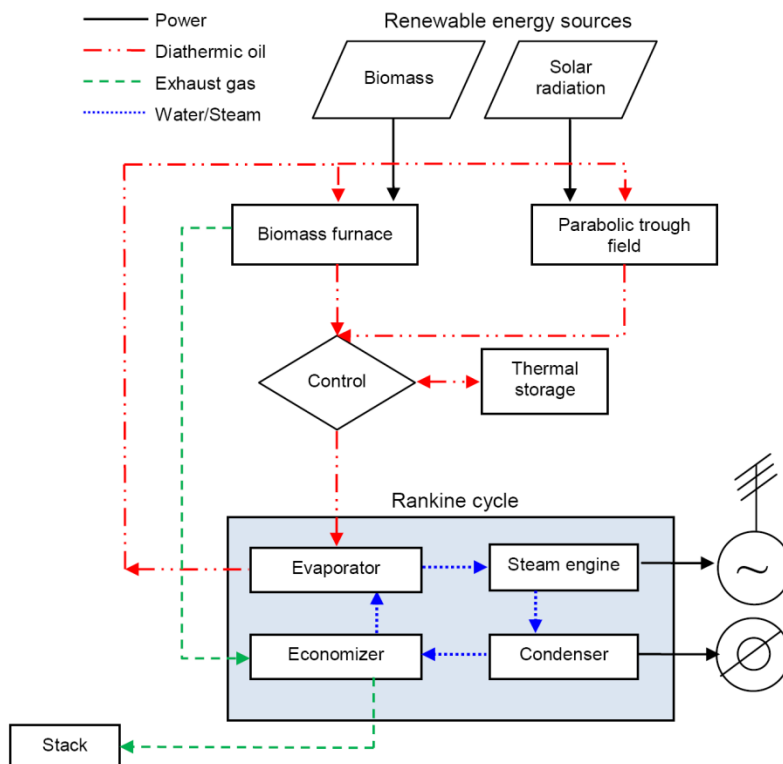**Figure 1.** Power plant diagram.

Table 1. Main components description and nominal size.

Component description		Size
Solar parabolic trough field (2,580 m^2)	kW$_{th}$	1,200
TES	GJ	57
Biomass furnace	kW$_{th}$	1,163
Reciprocating steam engine	kW$_{el}$	130
Condenser	kW$_{th}$	1,240
Diathermic oil circuit		
Maximum/minimum temperature	°C	300/240
Maximum/minimum specific heat	kJ/kg K	2.36/2.19
Operating pressure	kPa	800
Water/Steam circuit		
Maximum/minimum pressure	kPa	2,800/300
Maximum/minimum temperature	°C	230/134
Water/steam mass flow rate	kg/s	0.51
Electric power	kW	130
Thermal power	kW	1,100

The temperature-entropy diagram of the Rankine cycle is shown in Figure 2. The temperature-heat diagram is shown in Figure 3. The exhaust gas, diathermic oil and water-steam fluids are represented relating the reached temperatures with the Rankine cycle exchanged heat rate. In particular for the gas

produced by the biomass combustion two lines are plotted, one (Gas-35%) for the design condition with the biomass furnace working at 35% duty rate, and one (Gas-100%) for the fully biomass duty condition. The two extreme "gas "lines indicate the range of the solar contribution to the heat exchanges. The pinch point between the oil and water/steam lines is set equal to 10 °C.

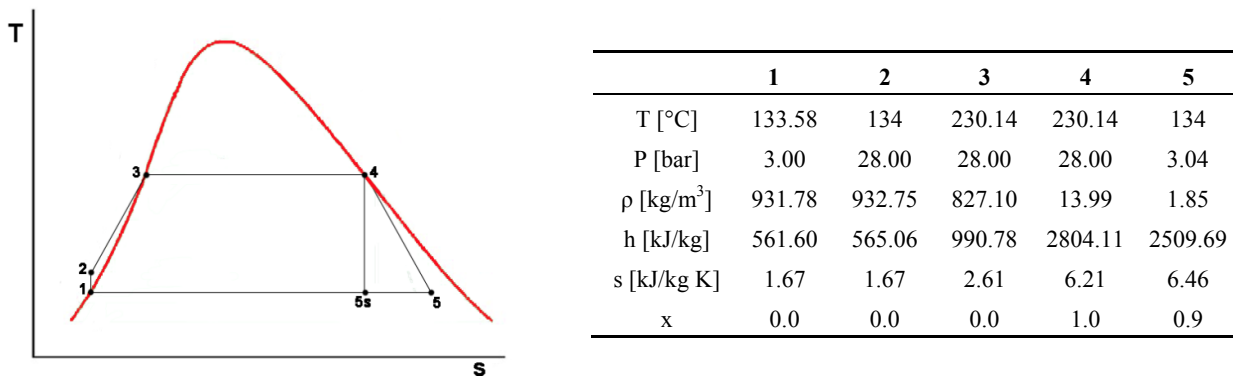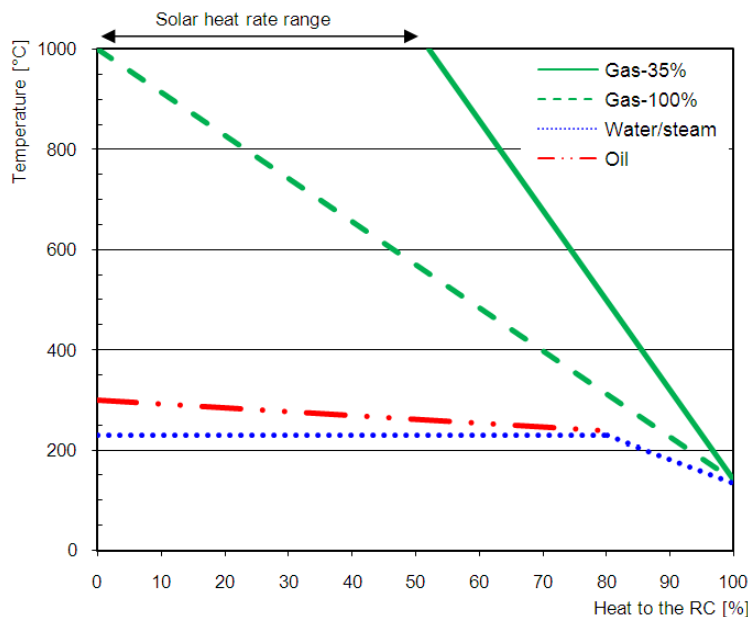**Figure 2.** Temperature-Entropy diagram of power cycle at reference state.

	1	2	3	4	5
T [°C]	133.58	134	230.14	230.14	134
P [bar]	3.00	28.00	28.00	28.00	3.04
ρ [kg/m³]	931.78	932.75	827.10	13.99	1.85
h [kJ/kg]	561.60	565.06	990.78	2804.11	2509.69
s [kJ/kg K]	1.67	1.67	2.61	6.21	6.46
x	0.0	0.0	0.0	1.0	0.9

Figure 3. Temperature-Heat diagram.

2.2. Transient Model Description

To evaluate the time-dependent behaviour and the performance of the proposed system a transient model was developed in the TRNSYS framework [22] integrated with the STEC library [23]. The RC transient model also includes in-house made types for the biomass furnace and for the reciprocating steam engine. The model subsets and their linkages are described by the flow diagram in Figure 4.

The CSP field works giving a constant temperature output of 300 °C by varying the HTF flow rate. In this circumstance the biomass furnace operates in parallel to the solar section, also supplying a variable flow rate at 300 °C.

Figure 4. Energy conversion system flow diagram.
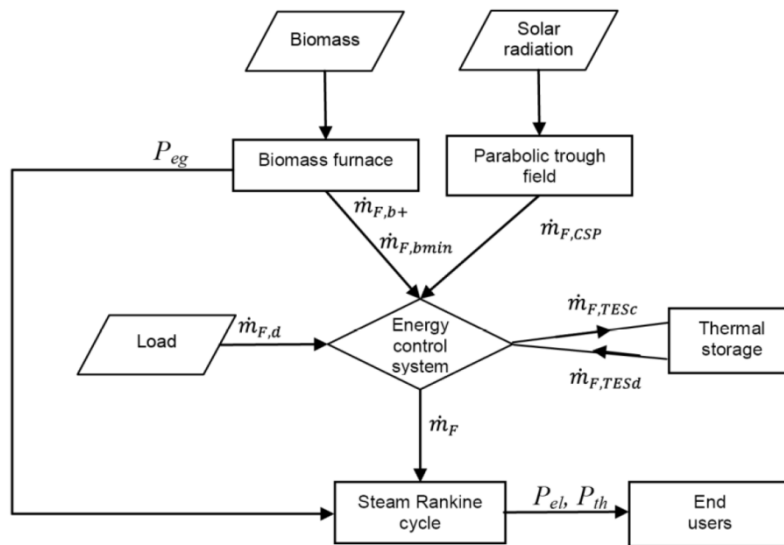
The model has been implemented by a control logic targeted to the tracking of different loads, namely heat or power demands. The development of the load tracking strategy has been based on the definition of algebraic correlations between the HTF flow rate, directly related to the RES power input, and the system thermal power output [P_{th}, Equation (1)] or the system electric output [P_{el}, Equation (2)], respectively. The HTF flow rate was selected as the reference parameter because it governs the actual power outputs according to the instantaneous renewable energy availability. A sensitivity analysis was carried out on the power system configuration by varying $\dot{m}_F$ and recording P_{el} and P_{th} values. During the sensitivity analysis the systems efficiencies were free to change. The effect of their variability is entailed in the obtained equations. Figure 5 shows the values obtained with the sensitivity analysis (grey lines) and the corresponding trend lines (dashed lines) and equations. The HTF control equations, accordingly derived, read as:

$$\dot{m}_F = 2 \cdot 10^{-6} \cdot P_{th}^{3.289} \tag{1}$$

$$\dot{m}_F = 3.6 \cdot 10^{-2} \cdot P_{el}^{2.713} \tag{2}$$

The control logic was implemented in order to match the requested HTF flow rate target ($\dot{m}_{F,d}$) at each time-step with the actual power demand according to the adopted load tracking law. Hence, the HTF flow rate target tracks the load evolution following a two-level control strategy, respectively driving the solar section and the whole system. In particular, the solar section control verifies the state of charge of the TES, giving priority to the storage charging in case of emptiness ($\dot{m}_{F,TESc}$). The flow rate not needed to charge the TES can be can be directly supplied to the Rankine cycle. The second control acquires the load data ($\dot{m}_{F,d}$) and compares the HTF flow rate target with the actual HTF flow rate achievable from the available solar field and the minimum biomass furnace rate ($\dot{m}_{F,bmin}$) at each time step, giving rise to three possible situations:

1. direct CSP contribution surplus, the exceeding HTF flow rate will first be sent to the TES (flow rate $\dot{m}_{F,TESc}$) and then dumped;
2. direct CSP contribution deficit, the missing heat flux will be first requested to the TES (flow rate $\dot{m}_{F,TESd}$); and

3. in case of insufficient flux from the solar section (flow rate $\dot{m}_{F,s}$) and minimum biomass contributions, an additional heat flux is requested to the biomass furnace (flow rate $\dot{m}_{F,b+}$).

Figure 5. (**a**) Thermal and (**b**) electric output control equations.

(**a**)   (**b**)
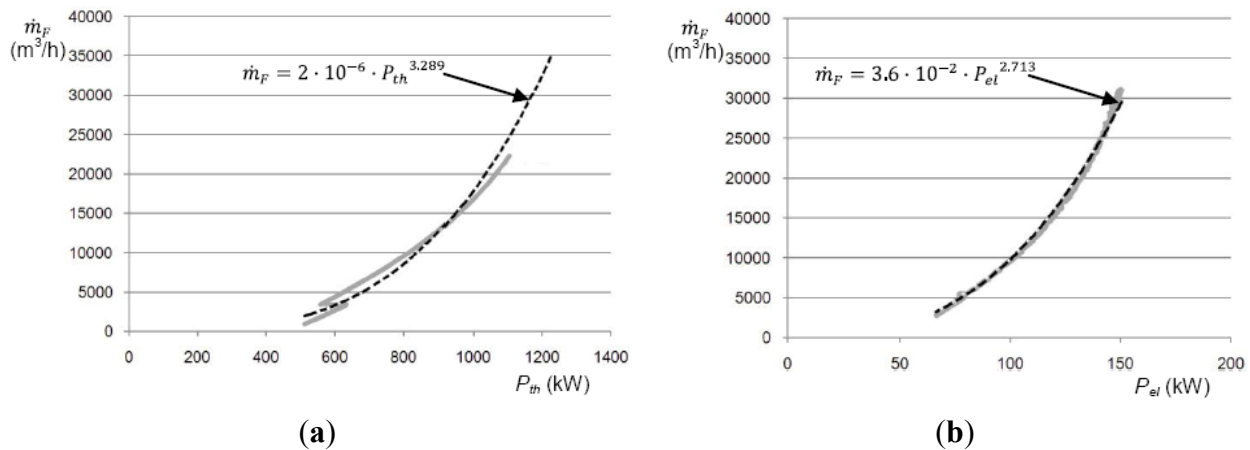
## 3. End User Description

3.1. End-User Load Profile

The behaviour of the proposed RES-based small-scale CHP Rankine cycle plant is investigated in the matching of load curve of a typical hotel end-user during a 24 hour time period. The hotel was chosen, among tertiary sector end-users, for its high annual heat/electricity consumption ratio. The end-user characteristics are summarized, in Table 2. The energy data gives a heat/electric consumption ratio higher than five, Table 2, which is typical of European hotel end-user figure, in contrast to the standard North-American hotel energy profile [28]. Furthermore, to take into account the cooling load also, it is worthy referring to the equivalent thermal load (obtained by the addition of the actual thermal load and the thermal load resulting if fulfilling the cooling load with an absorption chiller) with a 0.7 COP. In this case the heat/electric rises to a value of 7.44. The cooling load takes place only in the months from June to September, with a constant distribution of about 600 GJ/month.

Table 2. End users characteristics.

Type/Category	Business/leisure, 4 stars
Location	Industrial site
Activities	restaurants, bars, conference rooms, laundry
Number of rooms	190
Number of sleeping accommodations	350
Volume [m^3]	43,000
Area [m^2]	8,900
Heat load [GJ/y]	8,640
Electric load [GJ/y]	1,656
Cooling load [GJ/y]	2,580
Equivalent thermal load [GJ/y]	12,326
Heat/electric consumption ratio [GJ_{th}/GJ_{el}]	5.23
Equivalent heat/electric consumption ratio [GJ_{th}/GJ_{el}]	7.44

The thermal and electric load curves for a typical winter and summer day are shown in Figure 6. During the winter period, the thermal load ranges from 300 to 620 kW, with a sharp min-max modulation. On the other hand, the electric load (always below 100 kW) achieves its peak level in the morning and then it decreases during the day being nearly constant in the afternoon and evening times.

Figure 6. End user electric and thermal load for a typical (**a**) winter and (**b**) summer day.

(**a**)   (**b**)
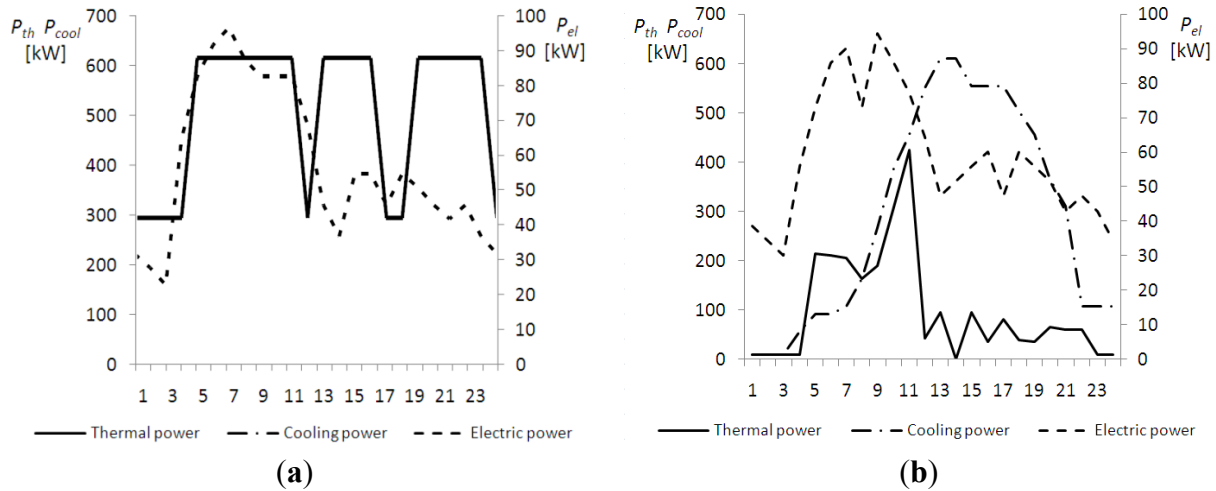
During the summer time, the thermal power achieves a peak of 425 kW during the morning while during the rest of the day it has an average value of 40 kW. The electric power load shape slightly differs from the winter one. In addition in summer a cooling power load is also present, concentrated during the afternoon hours. As previously stated, in the present study the cooling load is supplied by means of absorption chillers, thus in the following paragraphs it will be assimilated to a thermal load referring to as equivalent thermal load.

Figure 7. Hotel monthly (**a**) electric and (**b**) thermal load yearly behaviour. Left axis: monthly energy demand (●). Right axis: Variation of daily power request on monthly basis (I).

(**a**)   (**b**)
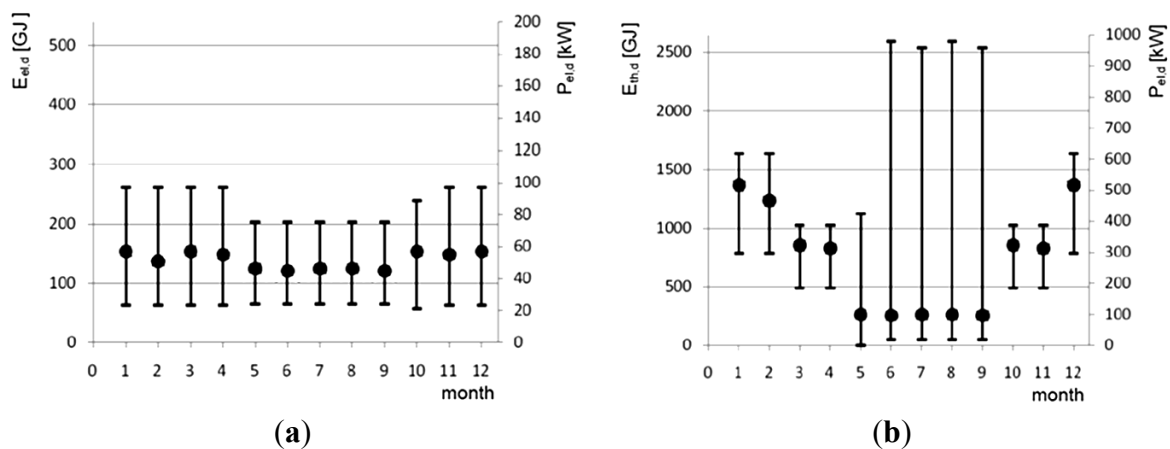
Figure 7 shows the monthly distribution of the electric and equivalent thermal load for the selected end-user; the monthly energy demand (●) is represented together with the power demand excursion (I). The electric energy request has an almost constant behaviour with monthly demand always below

200 GJ/day. On the other hand, the thermal monthly profile has a seasonal connotation which entails a thermal load range from 250 GJ on the summer period to 1,370 GJ on the winter one. It is worth noting that generally the average power demand is positioned on the lower part of the power demand excursion bars, indicating that the energy demand is composed by frequent low power demand values and rare high power values. This behaviour is highlighted in the summer equivalent thermal load curve (from June to September), when high peaks of cooling energy are requested during the day.

3.2. RES Data Input

The RES input data are available on a hourly distribution over a year period. The direct normal insulation data [29], are referred to Rome's latitude, *i.e.*, 41°54'39"24 N, as indicative of a central Italian location DNI data show a maximum value in the month of July, with 733.68 MJ/m^2 and a minimum value of 253.04 MJ/m^2 in December, with an annual cumulative irradiation of 5,760 MJ/m^2. Moreover, the ambient temperature has average yearly value of 15.71 °C, with a minimum of −7.4 °C in February and a maximum of 37.8 °C in August. The weather data on the selected winter day is shown in Table 3, providing the DNI and the dry bulb temperature hourly distribution.

Table 3. Direct normal insulation and temperature data for the selected winter day [29].

Hour	DNI [W/m^2]	Dry bulb temperature [°C]	Hour	DNI [W/m^2]	Dry bulb temperature [°C]
1	0	8.20	13	902.50	11.70
2	0	8.30	14	902.50	12.70
3	0	7.95	15	879.72	14.10
4	0	7.75	16	806.39	15.20
5	0	7.20	17	587.22	15.10
6	0	6.30	18	82.50	14.45
7	0	5.95	19	0.28	13.55
8	0.28	7.05	20	0	12.20
9	82.50	8.40	21	0	11.05
10	587.22	8.55	22	0	10.65
11	806.39	8.90	23	0	11.10
12	879.72	10.25	24	0	10.95

As far as the biomass is concerned, the thermo-chemical characteristics are typical of short rotation forestry derived woody pellet, with a lower heating value of about 17 MJ/kg and high carbon and oxygen ratios.

4. Solar-Biomass Power Plant Performance

The analysis of solar-biomass plant is based on the comparison of transient and overall performance under two power modulation scenarios: the tracking of the end-user thermal load in the hypothesis of electric energy surplus sale to the grid and, the tracking of the end-user electric load with a dump of the thermal energy surplus. It is worth noting that the present RC conversion system employs a reciprocating steam engine, which leads to a high thermal to electric energy ratio.

In the following, the overall CHP plant performances are first discussed analyzing the hourly data on a yearly and monthly basis. Afterwards, the study focuses on a typical winter day in order to discuss the behaviour of the system in operating conditions which are not favourable to the solar sub-system.

4.1. Overall Performance

In order to compare the performance of the solar-biomass CHP system under the two proposed load-tracking logics, a number of indicators have been considered (Table 4) concerning: the RES system performance, the energy output performance and the RC efficiency. The surplus and deficit index for the output performance were calculated by adding the surplus or deficit thermal and electric energy production which occurred any hour compared to the corresponding load energy request. The overall performances have been computed over a year period.

Table 4. Overall performance data.

		Electric Tracking	**Thermal Tracking**
RES system	Solar energy [GJ/y]	4,277.53	4,277.53
	Effective solar energy supply [GJ/y]	4,172.09	4,092.72
	Biomass energy [GJ/y]	18,132.39	17,221.31
	Solar fraction	18.71	19.20
	Biomass consumption [ton/y]	990.84	941.06
	Global effective energy input E_g [GJ/y]	22,304.48	21,314.03
Electric output	Plant electric energy output E_{el} [GJ/y]	2,064.37	2,017.10
	$E_{el,d}$ [GJ/y]	1,664.68	1,664.46
	$E_{el}/E_{el,d}$ [%]	124.01	121.19
	Surplus [%]	19.80	25.80
	Deficit [%]	−0.44	−8.32
Thermal output	Plant thermal energy supply E_{th} [GJ/y]	17,291.93	16,895.49
	$E_{th,d}$ [GJ/y]	11,656.13	11,653.99
	$E_{th}/E_{th,d}$ [%]	148.35	144.98
	Surplus [%]	40.09	33.27
	Deficit [%]	−7.49	−2.26
RC system	Net electric efficiency = E_{el}/E_g [%]	9.26	9.46
	Net thermal efficiency = E_{th}/E_g [%]	77.53	79.27
	Electric index = E_{el}/E_{th} [%]	11.94	11.94
	Primary energy ratio = $(E_{el}/\eta_{el} + E_{th}/\eta_{th})/E_g$ [-] [†]	1.21	1.24

[†] For the primary energy ratio evaluation, the values for the reference electric and thermal efficiencies are $\eta_{el} = 0.38$ and $\eta_{th} = 0.8$.

The integration over the duty time showed that the parabolic trough field collects 4,277.53 GJ/y of solar energy. Furthermore, as the energy input need varies in the two scenarios in reason of the different loads, the effective solar energy supply, which is a balance between the available solar energy and the TES charge/discharge rates, differs in the two cases with an amount of about 4,172 GJ/y in the electric tracking scenario and 4,093 GJ/y in the thermal tracking one. The biomass energy supply varies for the same reason, leading to an effective solar supply fraction (calculated as the percentage of the effective solar energy with respect to the sum of the effective solar energy and the biomass furnace

energy) of 18.71% in the electric tracking case and 19.20% in the thermal tracking one. Obviously, the solar energy production is strictly related to the size of the parabolic trough field. The selected sizing of the solar collector field is made in accordance to the Italian existing feed in tariff minimum size of 2,500 m^2 for the concentrated solar power.

Looking at the RC system performance Table 4, the value of 1.2 for the primary energy ratio demonstrates that the presented solar-biomass Rankine cycle systems can effectively allow the saving of conventional primary energy sources in each presented scenario. Looking at the electric output, globally the system produces more electric energy than the need with a peak production/request ratio of 124% for the electric tracking.

4.2. Hourly Power System Performance

The global data in a RES based plant are not indicative of the effective load covering. As a matter of fact, analyzing the hourly behaviour of the systems, there are both surplus and deficit situations. It is worth noting that in the hotel electric tracking scenario there are not thermal supply deficit occurrences. On the contrary, a 132% of thermal energy surplus is obtained. Considering that the electric source is easier to manage than the thermal one, as it can be sold or bought from the grid, the most suitable configuration appears to be the thermal tracking one.

Figure 8 shows the surplus (values higher than zero) and deficits (values lower than zero) behaviour of the electric and thermal power supply for both the electric and thermal tracking scenario. The graphs, presented on a monthly basis, are based on hourly data, and show, on the left axis, the minimum and maximum difference registered in the month between the load and the supplied power. On the right axis, the cumulative surplus and deficit energy is shown for each month. The electric output of the electric tracking configuration, Figure 8(a), shows the smaller values variation. Nevertheless, while this good result corresponds to the electric behaviour on the electric tracking configuration, the thermal behaviour is worse, with a high rate of surplus distributed all over the reference year and a deficit peak during the summer period, as the electric energy request is not sufficiently high to let the system to produce the requested thermal energy too. The deficit and surplus events have several explanations. The first one is that in both configurations one of the power output is a non tracked result, *i.e.*, when discussing the electric tracking configuration, the thermal output does not follow any production law, but is dependent from the electric production trend, without any correlation to the thermal load (and *vice versa*). Secondly, in most of the occasions the gaps with the requested load are entailed to the used correlation among load energy and hot thermal fluid flow rate, which do not perfectly fit the sensitivity analysis data, conducing to gaps between the desired output and the obtained one. Nevertheless, those gaps are not remarkable. The third reason, instead, is related to the high surplus peaks that occur when there are contemporarily an elevated available solar supply and full thermal energy storage. In those cases the system, which has to deliver the collected heat, sends the entire hot flow rate directly to the Rankine cycle. The last reason is related to the fact that the biomass furnace is always on duty, even if on a minimum rate, supplying energy also in extremely low energy request.

Figure 8. Hotel electric and thermal power surplus/deficit behaviour during a one year period under electric and thermal load tracking conditions.
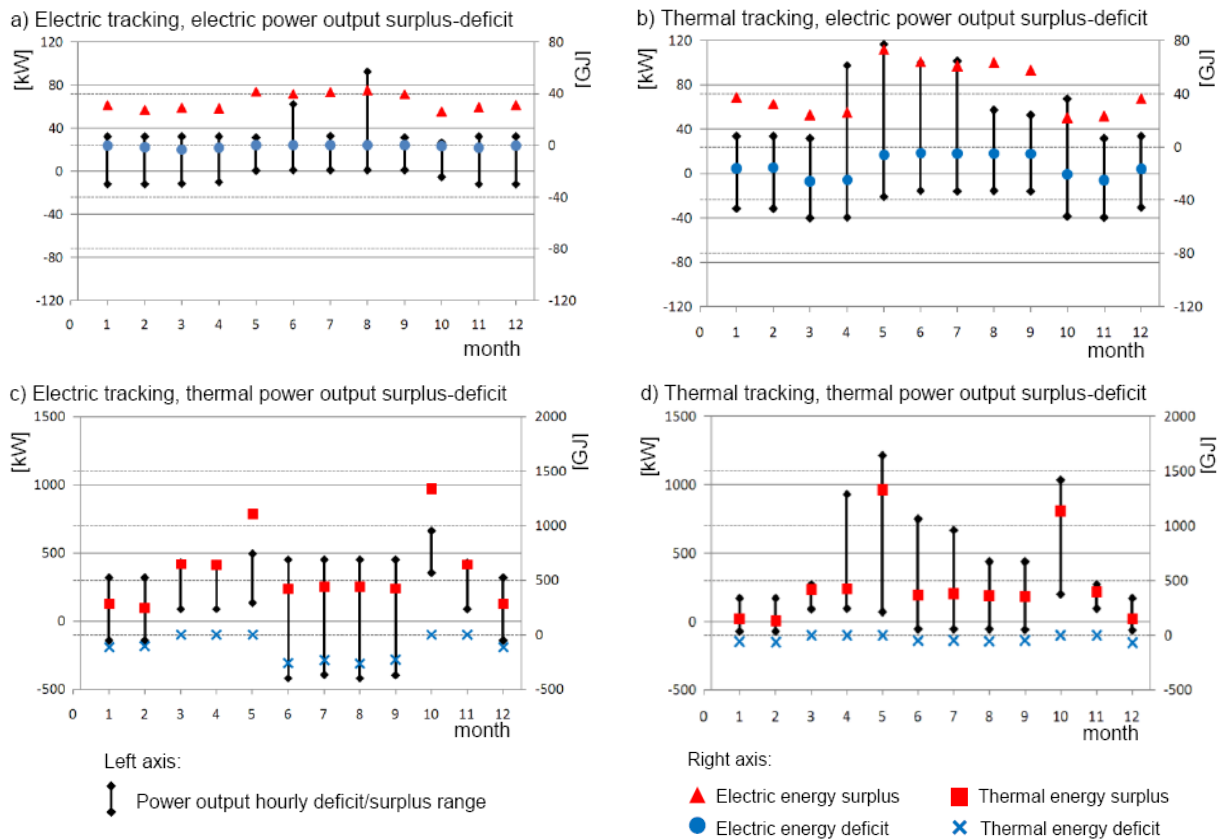
4.3. Matching Through the Load Tracking

The thermal and electric load tracking are analysed by comparing hourly distribution of the different power components. The thermal and electric load curves are shown in Figure 9. The thermal load ranges from 300 to 620 kW, with a sharp min-max modulation. On the other hand, the electric load, always below 100 kW, achieves its peak level in the morning and then it decreases during the day being nearly constant in the afternoon and evening times.

Figure 9. End user electric ($P_{el,d}$, right axis) and thermal ($P_{th,d}$, left axis) load for a typical winter day.
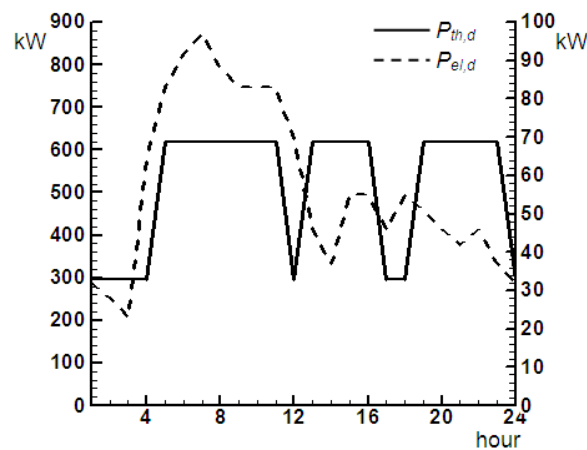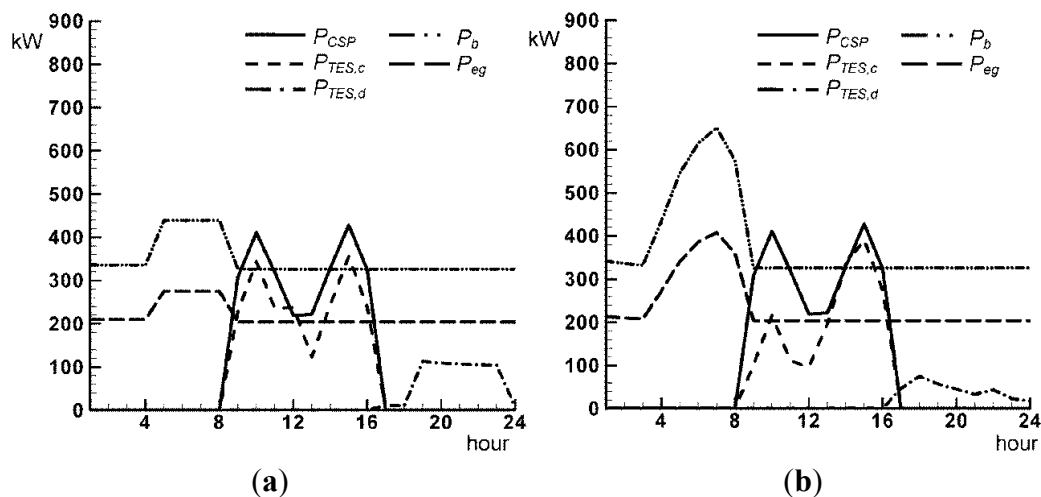
Figure 10 shows the power inputs to the RC, respectively from the solar field (P_{CSP}) and the biomass furnace (P_b), the TES contribution during the charge/discharge cycles ($P_{TES,c}$, $P_{TES,d}$), and the thermal power recovered from the exhaust gas (P_{eg}).

Figure 10. RES power contribution with the (**a**) thermal and (**b**) electric load tracking matching in the selected winter day.

(**a**)   (**b**)

As evident, the CSP power is available only between 8 a.m. and 5 p.m., with two peaks, respectively ante- and post-meridian, of about 400 kW. The P_{CSP} production shows a drop at midday. The reason of this behaviour, characteristic of the winter period, is the penalty coefficient [K(θ)] for the concentrating system optical efficiency depending on the solar radiation incidence angle influenced by the latitude of the site and the tracking axis orientation [30,31]. In this paper we selected a north-south tracking axis to maximize the collected energy.

In the thermal load tracking [Figure 10(a)] the P_{CSP} is not sufficient to meet the thermal load ($P_{th,d}$) which rapidly rises to its peak value about 600 kW (see Figure 9). For this reason the control system driven by the thermal demand, activates the TES system to discharge fractions of the solar energy ($P_{TES,d}$). The passage to the electric load tracking logic [Figure 10(b)] influences remarkably the RES power inputs/outputs and the TES charge/discharge cycle. In particular, the TES charge cycle is no more driven by solar radiation a.m. and p.m. peaks and it is shifted in the afternoon hours when the overall electric power request reduces. This circumstance causes the shifting of the TES discharge cycle to the evening time and unbalances the power input from the biomass furnace which is mainly concentrated in the early morning hours.

The matching of the power plant with the end-user demand, as driven respectively by the thermal and electric profile, is described in Figure 11 and Figure 12, by plotting the thermal power output (P_{th}) against the thermal power request ($P_{th,d}$) [Figure 11(a) and Figure 12(a)], and the electric power output (P_{el}) against the electric demand ($P_{el,d}$) [Figure 11(b) and Figure 12(b)].

In the thermal load tracking case, the thermal load ($P_{th,d}$) is almost completely satisfied by the solar-biomass plant output (P_{th}), Figure 11(a). The exceeding heat production during the periods of minimum request is consequent to the control regime of the biomass furnace which is kept at a constant minimum level. The missed production during the maximum request periods is due to tracking imperfections related to the adopted HTF control equations. When looking at the electric

matching, Figure 11(b), it is remarkable that the power plant electric output (P_{el}) mimics the shape of the leading load component. As a result, the correct sizing of the solar-biomass CHP system provides a fair matching in the period of peak electric request, while the load tracking logic drives the system to an over-production of electricity during the remaining duty time.

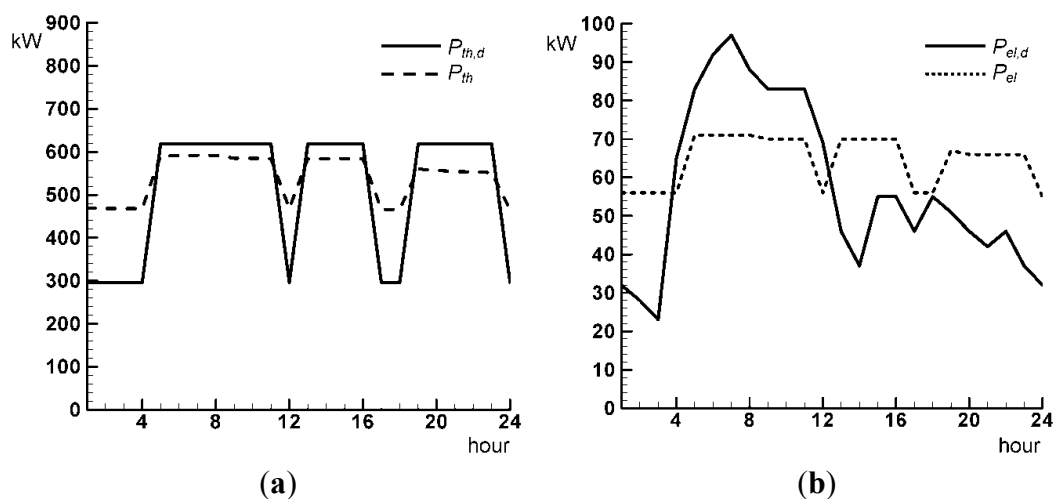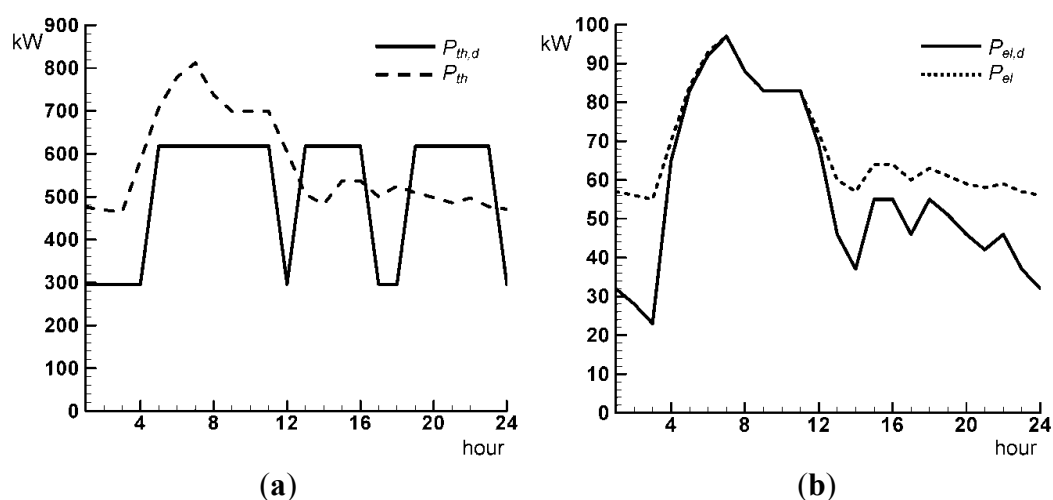**Figure 11.** (**a**) Thermal and (**b**) electric behaviour with the thermal load tracking matching for a typical winter day.

(**a**)   (**b**)

Figure 12. Thermal (**a**) and electric (**b**) behaviour with the electric load tracking matching for a typical winter day.

(**a**)   (**b**)

Looking at the electric load tracking case, Figure 12, the thermodynamic characteristics of the solar-biomass CHP system determine the significant overproduction of the thermal power output when the overall control is given to the electricity production. Figure 12(a) shows the electric peak request in the early morning which, giving rise to the intervention of the biomass, in absence of any direct or stored solar contribution, results in a surplus of heat availability. Moving to the electric matching, Figure 12(b), it is shown that the delivered electric power (P_{el}) follows fairly the load ($P_{el,d}$) between 4 a.m. and 12 p.m. while keeping it nearly constant in the remaining hours.

5. Environmental Issues

The potential and versatility of the plant demonstrate its suitability to work in an off-grid configuration, in both the electric and the thermal power tracking management. It is worth to assess environmental and economic aspects also. An effect of this system application are the entailed Greenhouse Gases (GHG) emission savings, estimated by means of emission factors related to the Italian thermoelectric power stations at reference year 2003. The emissions savings, Table 5, are evaluated considering the entire electric energy supply, in the hypothesis of grid transfer of the surplus, and the fraction of thermal energy supplied to the end users, in the hypothesis of dump of the thermal energy surplus. The result is a higher emission saving in the thermal tracking scenario, which avoids the emissions of about 3,400 ton/y of carbon dioxide, 3.59 ton/y of SO_x, 2.15 ton/y of NO_x and 0.14 ton/y of total suspended particles.

Table 5. Global emission savings.

	Electric tracking	Thermal tracking
CO_2 [ton/y]	2,967.87	3,442.71
SO_x [ton/y]	3.09	3.59
NO_x [ton/y]	1.85	2.15
TSP [ton/y]	0.12	0.14

Another essential environmental aspect is the net land use of the plant. Table 6 shows that the plant needs about 13,000 m^2. When including security distances and the space required for the power block, the needed surface amounts to about 31,000 m^2. Even if the solar field accounts for the 51.56% of the global footprint it is meaningful to reflect on the higher specific power of the parabolic trough field, *i.e.*, 0.46 kWp/m^2, when compared to the most commercial photovoltaic power plants (0.17 kWp/m^2) referring only to the devices surface area.

Table 6. Plant land use.

	Net land use
Solar field	6,780 m^2
TES	570 m^2
Biomass furnace, filter and stack	700 m^2
Biomass storage	3,000
Buildings (Rankine cycle elements, desalting units, offices)	2,100
Total	13,150 m^2

Concerning the costs, Table 7 indicates that the set of the parabolic trough field and the thermal energy storage is the most expensive device of the proposed system. In particular, the capital cost of a solar trough field with thermal storage has been estimated in 4,820 $/kW for the reference year 2006 [9]. It is worth noting that these data refer to large CSP technologies and must be considered only as a rough estimate of the present CSP device where the costs are presumably higher. Referring to the other technologies, the capital costs have been obtained by private communications with producers. Utilities entail costs for electric panels, electric and hydraulic connections, civil works, *etc*.

Table 7. Plant land estimated capital costs.

Technology	Cost [€]
CSP field with TES	7,870,000
Biomass furnace	130,000
Economizer	15,000
Evaporator	45,000
Steam engine	220,000
Condenser	15,000
Utilities	300,000
Total	8,595,000

Such high costs are constraining to the development of the proposed system when compared with the standard fossil fuel based power technologies. Nevertheless, in a fossil fuel free power generation perspective, the current high costs become a side issue in behalf of the sustainable development of the energy sector.

6. Conclusions

A model of a combined solar-biomass CHP plant devoted to feed a hotel end-user was presented. The well-established TRNSYS software was adopted for transient simulation. An analysis of thermal and electrical power production on a yearly basis demonstrated the feasibility of the present configuration in satisfying the energy requirements of the hotel.

The estimated energy output of the model was compared with the thermal and electric load in a winter day. The results for the two different load tracking scenarios were compared in terms of delivered power, matched load, RC system efficiencies and global GHG emission savings.

When looking at the output performance, the results show a most suitable behaviour for the thermal load tracking scenario, as it delivers both electric and thermal energy with less gap from the end-user requested energy.

The Primary Energy Ratio value of about 1.2 in both electric and thermal tracking cases indicates the capability of the presented system to save energy in comparison to two separated plants for the single electric and thermal energy production. Nevertheless, this configuration has high plant capital costs, *i.e.*, 7.2 k$/kW, that are mostly related to the solar section. Some interventions may be considering by adopting lower technology solar field, e.g., the passage from parabolic troughs to Compound Parabolic Concentrators (CPC) and the adoption of Direct Steam Generators (DSG) systems based on supercritical steam Rankine cycles.

References

1. Maidment, G.G.; Zhao, X.; Riffat, S.B.; Prosser, G. Application of combined heat-and-power and absorption cooling in supermarkets. *Appl. Energy* **1999**, *63*, 169–190.
2. Maidment, G.G.; Tozer, R.M. Combined cooling heat and power in supermarkets. *Appl. Therm. Eng.* **2002**, *2*, 653–665.
3. Brown, E.; Mann, M. *Initial Market Assessment for Small-Scale Biomass-Based CHP*; White Paper, NREL/TP-640-42046; National Renewable Energy Laboratory: Golden, CO, USA, January 2008.

4. Eastop, T.D.; Croft, D.R. *Energy Efficiency for Engineers and Technologists*, 1st ed.; Longman Scientific and Technical: Harlow, UK, 1990; p. 335.

5. Fröhlke, K.; Haidn, O.J. Spinning reserve system based on H2/O2 combustion. *Energy Convers. Manage.* **1997**, *38*, 983–993.

6. Kélouwani, S.; Agbossou, K.; Chahine, R. Model for energy conversion in renewable energy system with hydrogen storage. *J. Power Sources* **2005**, *140*, 392–399.

7. Corsini, A.; Rispoli, F.; Gamberale, M.; Tortora, E. Assessment of H_2- and H_2O-based renewable energy-buffering systems in minor islands. *Renew. Energy* **2009**, *34*, 279–288.

8. Sinden, G. *The Practicalities of Developing Renewable Energy Stand-by Capacity and Intermittency. Submission to the Science and Technology Select Committee of the House of Lords*; Environmental Change Institute University of Oxford: Oxford, UK, 2004.

9. *Assessment of Parabolic Trough and Power Tower Solar Technology Cost and Performance Forecasts*; NREL Subcontract Report 550-34440; Sargent & Lundy LLC Consulting Group: Chicago, IL, USA, October 2003.

10. *Solar Process Heat for Production and Advanced Applications*; Work Plan, IEA Solar Heating & Cooling Programme Task 49, Solar Paces Programme Task IV; International Energy Agency: Paris, France, October 2011.

11. Li, J. Scaling up concentrating solar thermal technology in China. *Renew. Sustain. Energy Rev.* **2009**, *13*, 2051–2060.

12. Al-Soud, M.S.; Hyayshat, E.S. A 50 MW concentrating solar power plant for Jordan. *J. Clean. Prod.* **2008**, *17*, 625–635.

13. Dong, L.; Liu, H.; Riffat, S. Development of small-scale and micro-scale biomass fuelled CHP systems. A literature review. *Appl. Therm. Eng.* **2009**, *29*, 2119–2126.

14. Badami, M.; Mura, M. Preliminary design and controlling strategy of small-scale wood waste Rankine Cycle (RC) with a reciprocating steam engine (SE). *Energy* **2009**, *34*, 1315–1324.

15. Borello, D.; Corsini, A.; Rispoli, F.; Tortora, E. Load Matching for a Combined Solar-Biomass Rankine Cycle Plant. In *Proceedings of the ASME-ATI-UIT Conference on Thermal and Environmental Issues in Energy Systems*, Sorrento, Italy, 16–19 May 2010.

16. Bohdanowicz, P.; Martinac, I. Determinants and benchmarking of resource consumption in hotels. Case study of Hilton International and Scandic in Europe. *Energy Build.* **2007**, *39*, 82–95.

17. Dalton, G.J.; Lockington, D.A.; Baldock, T.E. Feasibility analysis of renewable energy supply options for a grid-connected large hotel. *Renew. Energy* **2009**, *34*, 955–964.

18. Martínez-Lera, S.; Ballester, J. A novel method for the design of CHCP (combined heat, cooling and power) systems for buildings. *Energy* **2010**, *35*, 2972–2984.

19. Sanaye, S.; Raessi Ardali, M. Estimating the power and number of microturbines in small-scale combined heat and power systems. *Appl. Energy* **2009**, *86*, 895–903.

20. Papamarcou, M.; Kalogirou, S. Financial appraisal of a combined heat and power system for a hotel in Cyprus. *Energy Convers. Manag.* **2001**, *42*, 689–708.

21. Galvão, J.R.; Augusto Leitão, S.; Malheiro Silva, S.; Gaio, T.M. Cogeneration supply by bio-energy for a sustainable hotel building management system. *Fuel Process. Technol.* **2011**, *92*, 284–289.

22. Klein, S.A.; Beckam, W.A.; Mitchell, J.W.; Braun, J.E.; Evans, B.L.; Kummer, J.P. *TRNSYS—A Transient System Simulation Program*, *Version 15.1*; Solar Energy Laboratory, University of Wisconsin: Madison, WI, USA, 2000.

23. Schwarzbözl, P.; Eiden, U.; Pitz-Paal, R.; Jones, S. A TRNSYS model library for solar thermal electric components (STEC). A Reference Manual, 2002; Release 2.2.

24. Corsini, A.; Gamberale, M.; Rispoli, F. Assessment of renewable energy solutions in an Italian small island energy system using a transient simulation model. *ASME J. Sol. Energy Eng.* **2006**, *128*, 237–244.

25. Jones, S.A.; Pitz-Paal, R.; Schwarzboezl, P.; Blair, N.; Cable, R. TRNSYS Modeling of the SEGS VI Parabolic trough Solar Electric Generating System. In *Proceedings of the Solar Forum 2001: Solar Energy: The Power to Choose*, Washington, DC, USA, 21–25 April 2001.

26. Siangsukone, P.; Lovegrove, K. Modelling of a Steam Based Paraboloidal Dish Concentrator Using the Computer Source Code TRNSYS. In *Proceedings of the Solar 2002—Australian and New Zealand Solar Energy Society*, Newcastle, Australia, 27–29 November 2002.

27. Kolb, G.J.; Hassani, V. Performance of Thermocline Energy Storage Proposed for the 1 MW Saguaro Solar trough Plant. In *Proceedings of the ASME International Solar Energy Conference* (*ISEC 2006*), Denver, CO, USA, 8–13 July 2006.

28. *National Action Plan for Energy Efficiency Sector Collaborative on Energy Efficiency, Hotel Energy Use Profile*; EPA Summer Workshop Report; EPA: Washington, DC, USA, 2007.

29. SEL. Generated Hourly Weather Data. Solar Energy Laboratory, University of Wisconsin-Madison, 25 July 2003. Available online: http://sel.me.wisc.edu/trnsys/weather/generate.htm (accessed on 12 November 2008).

30. Manzolini, G.; Giostri, A.; Saccilotto, C.; Silva, P.; Macchi, E. A numerical model for off-design performance prediction of parabolic trough based solar power plants. *J. Sol. Eng. ASME* **2012**, *134*, 011003:1–011003:10.

31. Giostri, A.; Binotti, M.; Astolfi, M.; Silva, P.; Macchi, E.; Manzolini, G. Comparison of different solar plants based on parabolic trough technology. *Sol. Energy* **2012**, *86*, 1208–1221.